Cell

Four-Dimensional Imaging of *E. coli* Nucleoid Organization and Dynamics in Living Cells

Jay K. Fisher,[1] Aude Bourniquel,[1] Guillaume Witz,[1] Beth Weiner,[1] Mara Prentiss,[2] and Nancy Kleckner[1,*]
[1]Department of Molecular and Cellular Biology
[2]Department of Physics
Harvard University, Cambridge, MA 02138, USA
*Correspondence: kleckner@fas.harvard.edu
http://dx.doi.org/10.1016/j.cell.2013.04.006

SUMMARY

Visualization of living *E. coli* nucleoids, defined by HupA-mCherry, reveals a discrete, dynamic helical ellipsoid. Three basic features emerge. (1) Nucleoid density coalesces into longitudinal bundles, giving a stiff, low-DNA-density ellipsoid. (2) This ellipsoid is radially confined within the cell cylinder. Radial confinement gives helical shape and directs global nucleoid dynamics, including sister segregation. (3) Longitudinal density waves flux back and forth along the nucleoid, with 5%–10% of density shifting within 5 s, enhancing internal nucleoid mobility. Furthermore, sisters separate end-to-end in sequential discontinuous pulses, each elongating the nucleoid by 5%–15%. Pulses occur at 20 min intervals, at defined cell-cycle times. This progression includes sequential installation and release of programmed tethers, implying cyclic accumulation and relief of intranucleoid mechanical stress. These effects could comprise a chromosome-based cell-cycle engine. Overall, the presented results suggest a general conceptual framework for bacterial nucleoid morphogenesis and dynamics.

INTRODUCTION

Bacterial chromosomes are intriguing subjects for study. They are apparently "simpler" than their eukaryotic counterparts but nonetheless carry out all of the basic processes required for successful transmission of heredity, i.e., DNA replication and chromosome segregation in coordination with cell division. The present study investigates *E. coli* chromosomes from this perspective, focusing on the organization, organizational dynamics, and the dynamics of sister-chromosome segregation.

In eukaryotic organisms, sister segregation is usually discussed in terms of ropes and pulleys operating on compact, discrete objects: sister DNAs are organized initially into chromatin fibers and then into higher-order coherent shapes, all the while kept together by specific cohesin molecules. Sisters then segregate into well-separated spaces by the combined effects of progressive cohesin release and pulling forces generated by the mitotic spindle. Bacterial chromosomes, in contrast, spatially segregate sister chromosomes to opposite ends of the cell in the apparent absence of such apparatus. We have been interested to understand more about how this process might occur, in part because underlying principles might turn out to also be relevant to eukaryotic chromosomes.

For bacterial sister segregation, two general issues are important. First, the process of placing sisters in distinct spaces cannot be conceptually separated from the physical nature and organization of the nucleoid. At one extreme, it has been proposed that the nucleoidal fiber can be treated as a randomly oriented polymer, with sister fibers separated by the effects of entropic forces as they operate in the elongated space defined by the cylindrical cell periphery (Jun and Mulder, 2006). At the opposite extreme, sister nucleoid domains might comprise coherent, noninteracting entities that separate by mechanically pushing one another apart in space, with concomitant release of constraining intersister tethers (Bates and Kleckner, 2005; Joshi et al., 2011). Another model, where sister nucleoids are pumped outward in opposite directions from a "replication factory" (Lemon and Grossman, 2001; but see Bates, 2008), similarly necessitates an intrinsic tendency for nonintermingling of sister fibers. Yet, other models invoke centromere-like sequences that move via molecular motors along railroad tracks or are passively attached to the cell periphery on either side of midcell, with segregation driven by incorporation of cell-wall material at that site (Toro et al., 2008; Toro and Shapiro, 2010; Banigan et al., 2011; Norris, 1995). These latter models ignore the physical state of the nucleoid which, however, is probably highly relevant.

The second critical underlying issue for segregation of sisters is physical movement of nucleoid material which, in turn, requires energy. Where does this energy come from? Are thermal forces that are operating on a passive polymer fiber sufficient? Do molecular events place chromosomes in a high-energy, mechanically stressed conformation, which then drives ensuing segregation? Are ATP-driven processes directly involved in segregation and, if so, at which stages, by what mechanism, and in what type of interplay with intrinsic physical features and effects? To further address these questions, we developed

and applied a new experimental system for analysis of *E. coli* chromosome dynamics, at high resolution in time and in three-dimensional (3D) space.

RESULTS

Experimental System

Previous studies of nucleoid organization and structure have been limited by technical constraints. Analysis of fixed cells or isolated nucleoids has been informative but cannot detect dynamic behaviors. Also, the possibility of artifacts is always a concern. Analysis of living cells avoids fixation artifacts. However, light microscope imaging permits rapid image acquisition but provides very low spatial resolution while, oppositely, super-resolution methods give high spatial resolution but require data collection over timescales that preclude definition of rapid dynamic changes.

The current studies were carried out in living cells with a system that combines high spatial resolution and high temporal resolution (Figure 1; Experimental Procedures; Extended Experimental Procedures, available online). Nucleoids were visualized using the general nucleoid-associated protein HU, fluorescently tagged via its HupA subunit (HupA-mCherry) and imaged by wide-field epi-fluorescence microscopy. Imaging provides spatial resolution of less than 260 nm in the XY dimension and less than 470 nm in the Z dimension. An entire nucleoid can be imaged in 3D by a series of Z stacks (Figure 1B) in as few as 2 s. Successive 3D images of a single nucleoid can be taken as frequently as once every 5 s. Concomitantly, the boundaries of the cell periphery are accurately defined for the midcell plane from phase-contrast images (Figure 1A, bottom).

For maximum spatiotemporal resolution, cells were imaged while growing in microfluidic channels, wherein they are immobilized by gentle "hugging" in the Z dimension (Figures 1A, top, and S1A–S1D). Growth medium still flows continuously around the immobilized cells. These cells progress through the cell cycle with the same kinetics as occur in exponential phase growing under the same conditions in a standard liquid culture.

Importantly, this analysis utilized a strain background and growth conditions where events of the chromosome cycle have previously been analyzed in detail by other methods (CM735; Bates and Kleckner, 2005; Bates et al., 2005; Joshi et al., 2011). Under these conditions, cells grow in an ~120 min "linear" cell cycle. Cell division is followed by a ~10 min "G1" period. DNA replication is then initiated. Replication lasts ~60 min. An additional ~50 min then elapses prior to the next cell division.

A final key aspect of this study is that *oriC* dynamics were analyzed by FROS, in parallel with whole-nucleoid dynamics. Separation of sister *oriC*s from one another is an easily discerned event that occurs after initiation of replication, at a specific time in the cycle (Figure S1G) (Bates and Kleckner, 2005). This event provides a fixed point of reference for defining the timing of events in any particular nucleoid and for temporal alignment of different independent nucleoids.

Features of interest were confirmed in another strain background, with another fluorescent nucleoid-associated protein, and/or in cells imaged outside of channels and in the absence of flow, as detailed below.

The G1 Nucleoid Is a Discrete, Helical Ellipsoid

3D imaging reveals that G1 nucleoids are well-defined ellipsoids that exhibit a variety of helix-like forms (e.g., Figures 1C and 1D and Movie S1; hereafter referred to as "helical" for simplicity). This shape is clearly defined after one round of deconvolution, which eliminates out-of-focus information without introducing artificial sharpening or enhancement, but it is also visible in raw images (Figure S1E).

The longitudinal paths of G1 nucleoids can be evaluated by slicing each 3D data set into a series of cross-sections perpendicular to the long axis of the nucleoid and computationally defining the density centroids of these slices. The paths of these centroids exhibit left- and/or right-handed helicity even along the length of a single nucleoid (Figure 1D). Thus, the important feature of nucleoid shape is the tendency for curvature, not any particular handedness.

HupA-mCherry fluorescence intensity reports nucleoid DNA density, not peculiarities of HupA binding or the disposition of free HU protein. The same basic nucleoid shape is observed in fixed cells where the nucleoid is illuminated by nonspecific binding of SSB-GFP to single-stranded DNA regions created by the preparation procedure (Figure S1H) and in living cell nucleoids illuminated by FIS-GFP (Figure S1J). Also, helical shape is observed in cells growing outside of channels on agarose pads in the absence of flowing medium (Figures S1J, 2F, and 3C–3K) and in cells removed from synchronous liquid cultures and imaged within minutes after attachment to a glass slide (unpublished data, A.B.).

Comparison of fluorescence nucleoid images and phase-contrast midplane images (e.g., Figure 1H, ivory and green, respectively) further reveals that, at early G1 (left panel) the nucleoid is closely juxtaposed to the cell periphery in the radial dimension along its entire length but is well separated from the old pole end of the cell, as previously inferred from fixed cell studies (Bates and Kleckner, 2005). Separation from the old pole end of the cell can be even more pronounced at later stages (further examples below; Figures S2A and S2C). This same disposition has been observed in cells grown on agarose pads and imaged with FIS-GFP (Figure S2F). The same two features are also apparent in 3D STORM images of mEos2-labeled HU, which provide higher spatial resolution, but lower temporal resolution, than those of the current study (Wang et al., 2011). Thus, the nucleoid does not simply fill up the interior cell space; rather, it is a discrete, internally delimited object.

The space at the end of the cell, while certainly containing proteins and small molecules, is nonetheless fully accessible to the nucleoid, rather than being solidly occluded by ribosomes or other nonvisualized cellular components, because (1) the nucleoid *does* extend to the ends of the cell at some stages, as shown below by analysis of post-G1 nucleoids; (2) plasmid DNAs localize beyond the nucleoid at the ends of the cell (Kuhlman and Cox, 2012); and (3) at some stages, individually tagged chromosomal loci explore the space beyond the end of the nucleoid (J.K.F. and A.B., unpublished data).

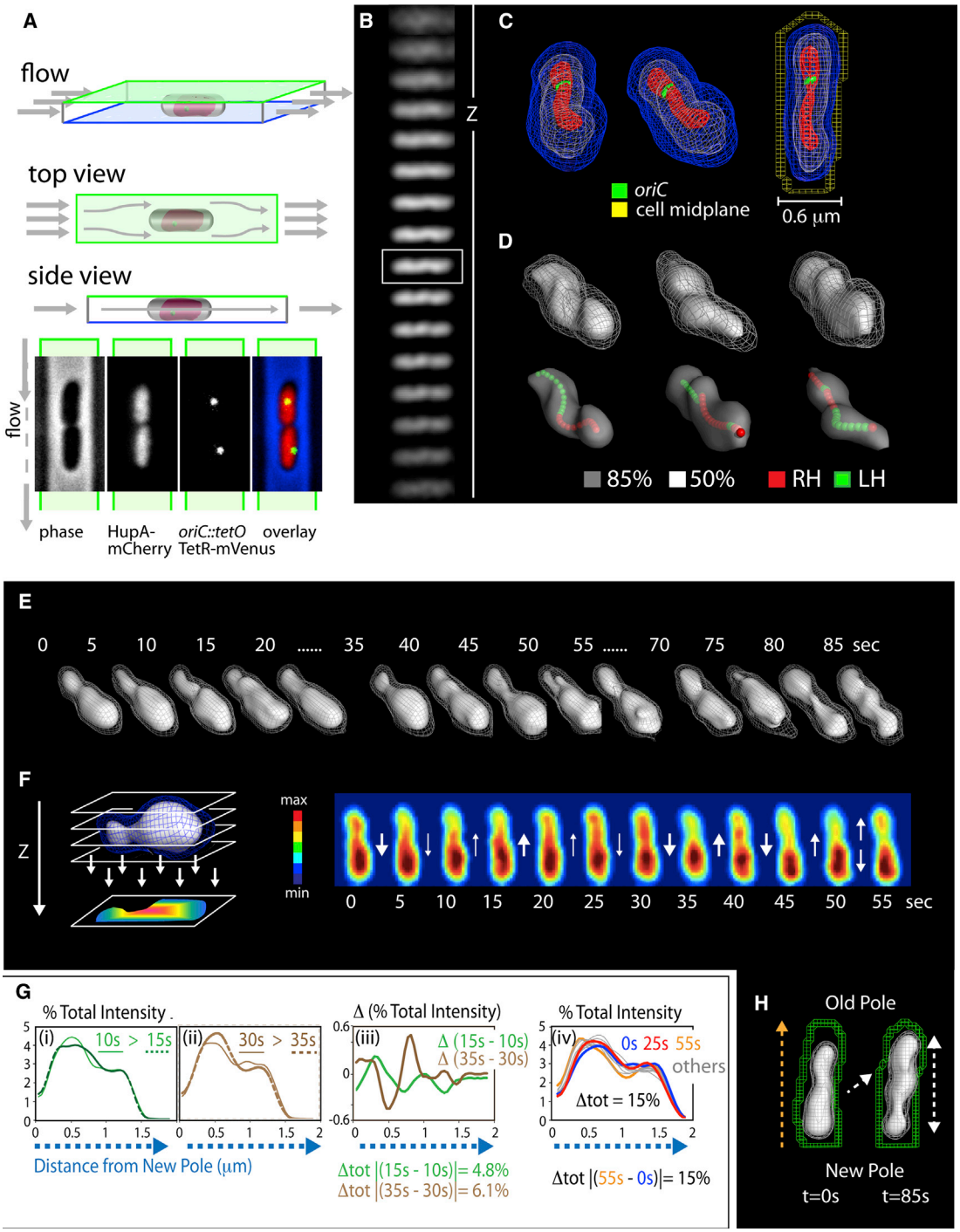

Figure 1. The G1 Nucleoid Is a Discrete but Dynamic Helical Ellipsoid

(A) Top: Normally growing *E. coli* cells were imaged in microfluidic chambers, held in place by gentle hugging in the Z dimension, with fluid flowing around both sides. Bottom: The cell periphery, nucleoid and desired FROS foci (here marking *oriC*) were imaged by phase contrast and wide-field epifluorescence, in 3D, via collection of successive Z stacks over less than 2 s.

(B) Z stack of HupA-mCherry images; nucleoid dimensions are 1.64 μm by 0.48 μm.

(C) Isointensity PyMOL reconstruction of a G1 nucleoid, alone and with cell midplane outline (total signal [blue] and 50% and 20% of total signal [red and white]). The helical ellipsoid fills the cell radially but does not contact the cell at its new pole end. Radially decreasing signal intensity suggests radially decreasing density, subject to imaging resolution limits.

(D) Isointensity reconstructions and longitudinal density centroid paths for three nucleoids; curvature handedness of curvature in red and green. Left-most nucleoid is that in (B).

(legend continued on next page)

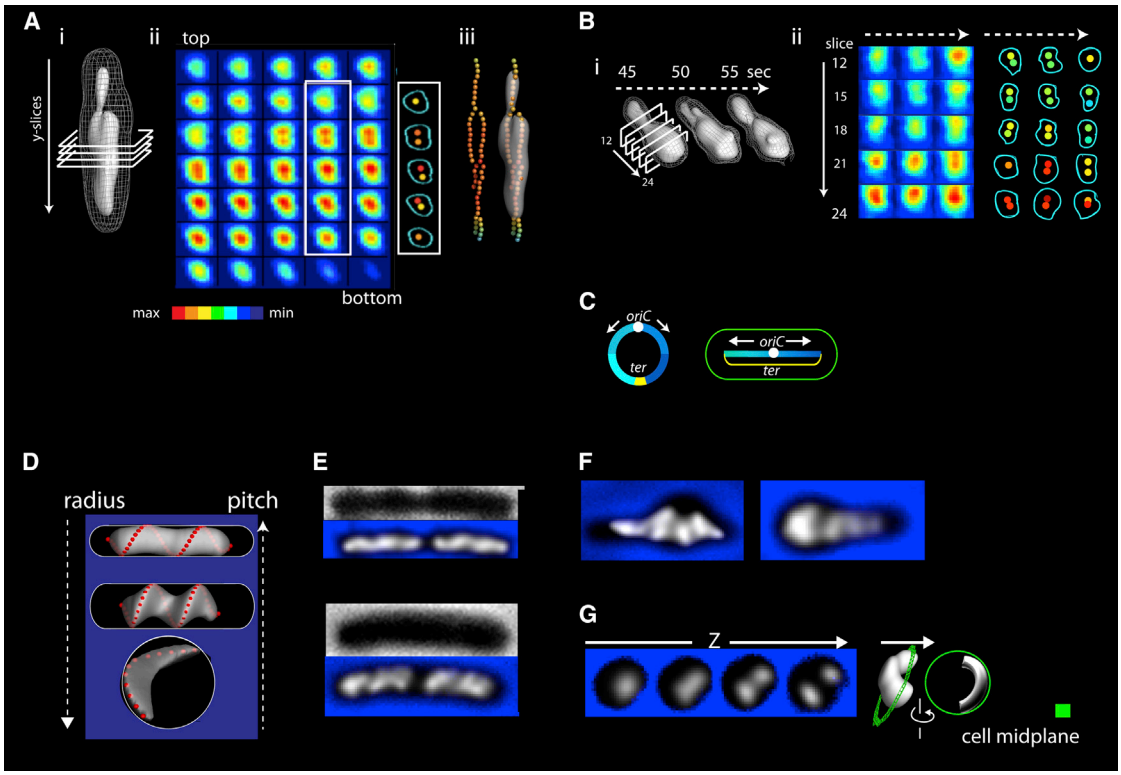

Figure 2. Nucleoid Substructure Comprises Dual Longitudinal Density Bundles

(A) Cross-sections of a G1 nucleoid (i) displayed in a color-coded array (ii). Dual longitudinal density bundles are revealed. Central densities occur along the nucleoid in continuous paths with a tendency for relational coiling (iii).

(B) Bundle patterns change position, intensity, and extent of duality in accordance with changes in nucleoid shape as seen at 5 s intervals.

(C) Most of the *E. coli* G1 genome is arrayed linearly from one end of the cell to another, with the ~300 kb terminus region stretched between the two nucleoid ends. Thus, G1 duality is not genomically specified. Images in (A) and (B) from 1 × deconvolved data.

(D–G) A change in cell radius results in a concomitant change in nucleoid helical radius and an inverse change in nucleoid helical pitch.

(D) Predictions expected for a longitudinally stiff ellipsoid that is deformed into a helical shape by radial confinement.

(E–G) Variations that match the predictions in (D) are observed in three cases.

(E) Two different living cell types.

(F) One hundred minute growth in the presence of cell-wall-synthesis inhibitor mecillinam causes rounding up of cells at their (emerging) poles with changes in helical parameters in the expanded region.

(G) Ten minutes after spheroplasting by cell-wall removal yields open low-pitch crescents. Images (E–G) are from 20 × deconvolved data to emphasize shape.

Since we can specifically define the limits of the nucleoid, we can further define additional features. First, all detectable HupA-mCherry intensity is involved in the shape (Extended Experimental Procedures). Second, nucleoid DNA density is very low: the atoms of the DNA duplex take up only ~2% of total cell volume while the nucleoid shape comprised of this DNA occupies ~75% of the total space (see Extended Experimental Procedures).

The G1 Nucleoid Is Highly Dynamic Due to Oscillating Longitudinal Density Waves

G1 nucleoid shape is highly dynamic. Significant global changes are apparent over intervals as short as 5 s (e.g., Figure 1E and Movie S2). Furthermore, when total nucleoid density is summed in the Z dimension (Figure 1F, left), shape changes are seen to result from waves of density that flux longitudinally, up and down the shape, over distances comparable to the length of

(E–H) Dynamic shape changes via longitudinal density waves in a single nucleoid imaged at 5 s intervals.

(E) 3D isointensity shape reconstructions.

(F) Nucleoid intensities were summed by projection in the Z dimension (left). Color map representations (right) reveal rapid longitudinal fluxes of density over distances comparable to nucleoid length.

(G) Nucleoid intensities of cross-sectional slices along the length of the nucleoid (percentage of total intensity as a function of slice position), at the indicated time points (i, ii, iv). (iii) For pairs of time points, the difference in intensity at each position/slice is calculated and absolute values of these differences summed for all slices.

(H) The nucleoid in (E)–(G) in relationship to its cell midplane at the beginning and end of the time series. Green shapes are the cell periphery in the midplane section of the corresponding phase-contrast image; ivory shapes are suitably oriented isointensity reconstructions. Flat bottom end to cell outline reflects close juxtaposition to its sister cell; the junction was approximated by a straight line. All images from 1 × deconvolved data.

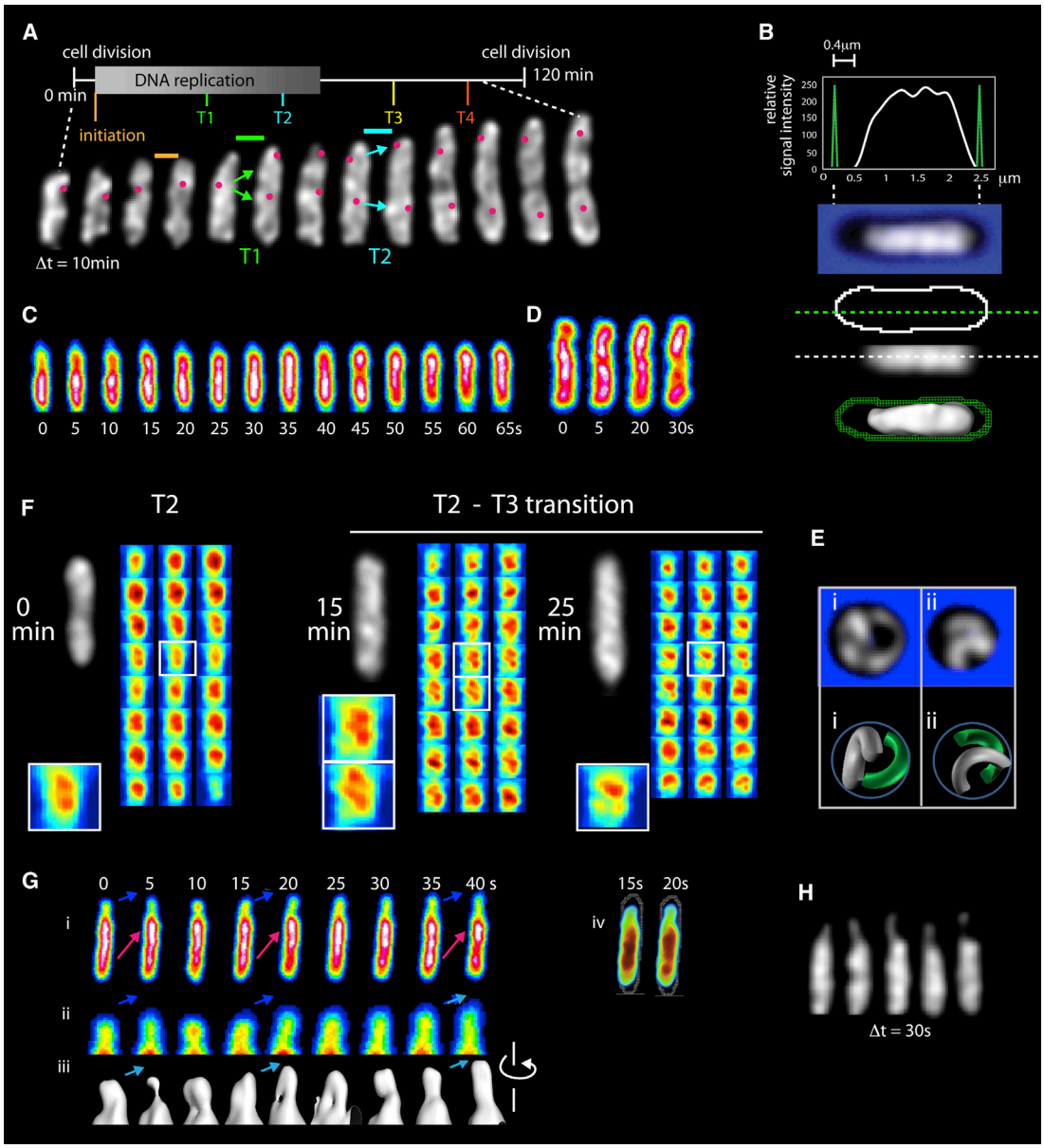

Figure 3. Post-G1 Nucleoids

(A–F) Basic features of G1 nucleoids also occur at later stages.

(A) A single nucleoid imaged at 10 min intervals reveals progressively evolving helix-like shapes with radius and pitch analogous to those at G1. Four transitions (T1–T4). Diagnostic origin movements at T1 and T2 are documented by concomitant imaging of *oriC*. Fully individualized sister nucleoids emerge only at the very end of the cell cycle (after completion of this imaging series).

(B) Post-G1 nucleoids fill the cell radially but often, as in this case, do not come close to the old pole end of the cell (as in Figure 1C; also Figure S2).

(C and D) Longitudinal density waves occur during DNA replication (C) and after completion of replication (D) (as in Figure 1F; quantification in Figure S3B).

(E) Spheroplasting of a late-stage cell creates low pitch crescents (as in Figure 2G; Z series in Figure S4). Maximal separation implies a tendency for nonintermingling.

(F) Longitudinal density bundle patterns (as in Figures 2A and 2B) for the same nucleoid at successive times in the T2 to T3 period, showing duality (left), a multiple-bundled state (middle), and a peculiar midcell pattern (right). The latter two morphologies are not seen in G1 nucleoids.

(G) Elongation of a post-G1 nucleoid seen by imaging at 5 s intervals. Z projections illustrate protrusion of nucleoid density into empty space at the old pole end of the cell (blue arrows in i and ii) with accompanying longitudinal density waves that move up and back through the shape in the same direction (i; red arrows) analogously to an incoming tide. Isointensity PyMOL thresholding of the same nucleoid (iii) reveals dual longitudinal density bundles in tightly juxtaposed or open states. Variations in thickness reveal incorporation of fluxing density into the shape. (iv) 3D PyMOL rendering of the same nucleoid illustrating protrusion of density into nucleoid-free space at the old cell pole.

(H) Midplane images, taken at 30 s intervals, of a nucleoid exhibiting a long, thin protruding finger that is curving around the radial cell periphery with concomitant density fluxes. All images from 1 × deconvolved data.

the nucleoid, with apparent periodicities of seconds-to-minute(s) (Figure 1F, right). These "longitudinal density waves" are fluxing through the nucleoid in 3D to generate shape changes. Relatively modest changes in nucleoid density distribution are involved. Between images taken 5 s apart, ~5%–10% of total intensity shifts position (Figure 1G, i–iii) with shifts of ~15% over longer intervals (Figure 1G, iv).

Longitudinal density fluxes are a general, robust feature of nucleoid dynamics. Such fluxes have been observed in each of approximately twenty 5 s time series of G1 or G1/S transition nucleoids and each of ~100 time series of nucleoids at other cell-cycle stages. Six G1 nucleoids and six G1/S nucleoids, each imaged over periods of ~40 s, exhibit average density shifts per 5 s interval of 7.2% and 6.6%, respectively. Furthermore, in G1 nucleoids of cells expressing both HupA-mCherry and FIS-GFP, both signals exhibit the same density waves (Figure S3A), which thus represent changes in underlying nucleoid density, not fluxes of HU or FIS protein alone, irrespective of the nucleoid. Density waves are also seen in cells growing on agarose pads without flowing medium and thus are not due to confinement in microfluidic channels nor to fluid flow past tethered or confined cells. Finally, density fluxes are not observed in fixed cells (Figures S3C–S3K) and thus are not artifacts of imaging or image processing.

These findings reveal the existence of short-timescale chromosomal motion. This motion occurs prior to onset of DNA replication (and after completion of replication, as shown for analysis of post-G1 nucleoids below) and thus is replication independent.

Previous studies show that G1 nucleoids also undergo coherent, longer timescale, globally directional motions. During and immediately following cell division, nucleoids are closely juxtaposed to the evolving new poles at midcell (Bates and Kleckner, 2005), with asymmetric shapes that are fatter at the new pole end (e.g., Figure 1H, left). This configuration probably reflects molecular linkages between the pole and the terminus (*ter*) macrodomain (Espéli et al., 2012). As septum formation is completed, sisters move away from the emerging poles, without major internal reorganization but with concomitant elongation (Bates and Kleckner, 2005; Figure 1H, right). Time-lapse further reveals that elongation concomitantly yields a more regular shape with a more even density distribution (e.g., Figure 1H, compare left versus right). Longitudinal density fluxes presumably underlie these movements. However, these fluxes must in some way be directionally biased so as to give the observed effects (Discussion). Additionally, the G1 nucleoid retains its close contact with the cell periphery throughout dynamic shape and length changes (e.g., Figure 1H).

The G1 Nucleoid Has a Substructure Comprising Dual Longitudinal Density Bundles

When cross-sectional slices perpendicular to the length of the nucleoid (Figure 2A, i) are displayed in an intensity-coded array (Figure 2A, ii), density substructure is revealed. Some slices exhibit a nearly symmetrical "bulls-eye" pattern; however, many exhibit two structures of high central intensity, one stacked above the other. The same features characterize fully individualized sister nucleoids immediately prior to cell division (pre-G1). Doubleness is seen in nondeconvolved images and thus is not a deconvolution artifact (Figure S1I).

The dual-density centroid(s) of cross-sectional slices run continuously along the length of the nucleoid (Figure 2A, iii). We thus describe the revealed subshapes as longitudinal density bundles. In accordance with the fact that they underlie an ellipsoid shape, bundles are wider in the middle of the nucleoid than at the ends. In accordance with the helical shape of the ellipsoid, dual-bundle paths tend to be relationally twisted (Figure 2A, ii and iii). And since the entire nucleoid is involved in the helical ellipsoid shape and its component density bundles, the nucleoid does not comprise a central scaffold surrounded by disordered material.

Further, in accordance with dynamic nucleoid shape changes, bundle patterns change in intensity and position as density waves flux through the nucleoid (Figure 2B). These dynamics probably reflect local changes in interfiber proximity rather than global movement of a fixed proteinaceous core (Discussion).

Intriguingly, G1 nucleoids are single genomes; no sister is present. Moreover, while the *E. coli* chromosome is a single circular DNA molecule, ~95% of the genome is linearly organized along the cell length, with a thin, elongated strand completing the circle (Figure 2C) (Wang et al., 2006; Wiggins et al., 2010). This organization was defined in AB1157, which, we show, also exhibits dual longitudinal bundles at G1 (Figure S1F). Thus, dual bundles do not reflect the "left" and "right" sides of the circular chromosome but instead imply the existence of an intrinsic tendency for duality (or more generally, "splitting") due to some biochemical and/or physical feature of the system.

Nucleoid Radius and Nucleoid Pitch Are Both Defined, Inversely with Respect to Each Other, by the Cell Radius

The nucleoid is in close contact with the cell periphery. We further find that a change in the radius of the cell confers both a matching change in the helical radius of the nucleoid plus an inverse change in nucleoid helical pitch (Figure 2D) in three types of studies. (1) The standard strain for this study exhibits spontaneous variation between two cell types, longer/thinner and shorter/fatter, whose nucleoids respectively exhibit smaller radius with greater pitch and larger radius with smaller pitch (Figure 2E). (2) Inhibition of cell-wall synthesis causes rounding-up of midcell regions where, locally, the nucleoid exhibits increased radius and decreased pitch (Figure 2F). (3) Enzymatic cell-wall removal, carried out in the absence of DNA-condensing agents converts the cell to a spherical shape and, concomitantly, the nucleoid becomes a very large radius, low-pitch ellipsoidal crescent, still juxtaposed against the edge of the cell (Figure 2G).

These observations imply that helicity of the nucleoid shape is not determined internally (e.g., by the longitudinal density bundles described above); instead, the helical aspect is determined by interaction of the basic ellipsoid form with the radial cell periphery. Further, since cells become spheroplasts by cell-wall removal in only a few minutes, such interaction is required not only to establish helical dimensions but to maintain those dimensions.

Strikingly, the observed correlations are precisely those predicted if the nucleoid is a longitudinally stiff ellipsoid that has been forced into a helical path within a too-small cylinder

(i.e., a cylinder whose radius is smaller than the persistence length of the ellipsoid). If the nucleoid could be forced into a radially confined helical shape as it evolves, the resulting state could then be maintained by outward-directed pushing forces along the nucleoid length.

The observed effects might be explained, alternatively, if the nucleoid were a soft ellipsoid that was linked to the inner cell periphery specifically along a peripheral helical path (red dots in Figure 2D). We do not favor this model because (1) the nucleoid does not exhibit a tightly defined external helical-peripheral path that would encourage such association; (2) the nucleoid is of relatively low density around its entire outer surface, implying that molecular contacts between the nucleoid and cell periphery strong enough to change the shape of the nucleoid would probably rip the nucleoid apart; and (3) contrary to early reports, there is no continuous peripheral-helical cytoskeleton to which the edge of the nucleoid might attach (Swulius and Jensen, 2012).

All Described Features of G1 Nucleoids Are Also Present during and after DNA Replication

After G1, nucleoids exhibit helical shapes that evolve over time (Figure 3A). Under the conditions analyzed, the cell cycle is demarked by four transitions (Figure 3A; further discussion in the following section). Among these, T1 and T2 are accompanied by diagnostic *oriC* dynamics (Figure S1G; details in following section).

The nucleoid elongates throughout the cell cycle, during and after DNA replication; moreover, fully morphologically individualized sister nucleoids do not emerge until the very end of the cell cycle, long after completion of DNA replication (Figure 3A). Post-G1 shapes often comprise multiple helical turns and can be ellipsoidal, with elongated ends, or can have openly curved ends (Figure 3A).

Post-G1 nucleoids exhibit all features described above for G1 nucleoids, both during replication and during the lengthy ensuing postreplication predivision period, as follows: (1) Nucleoid helical radius corresponds to cell radius, with radius and pitch both closely similar to those seen at G1 (Figure 3A). (2) The nucleoid is always in contact with the radial cell periphery, but is often far from the old pole end of the cell, particularly at the T1/T2 transition (Figures 3B and S2; following section). (3) Longitudinal density waves occur in all nucleoids, during and after replication, as documented by 5 s time-lapse analysis of ~100 nucleoids representing the entire cell cycle (e.g., Figures 3C and 3D). (4) Cell radius defines both nucleoid radius and pitch, in inverse correlation (Figures 3E and S4). Cells at quite late stages, rendered spherical by cell-wall removal, exhibit pairs of nucleoids, each with greatly increased curvature and greatly decreased pitch. Additionally, the two nucleoids are disposed so as to minimize overlap, suggesting that they are intrinsically discrete, nonintermingling objects (Figures 3E and S4; Discussion). (5) Nucleoids exhibit longitudinal density bundles that are often split. Bundle duality is common at all stages (e.g., Figure 3F, left), including pre-G1 (Figure S5B). Moreover, in the latter stages of DNA replication, interesting morphologies occur that are not seen at other stages. In the example shown, a single nucleoid exhibits duality just after the T2 transition and then, during the run-up to T3, first exhibits three (or more) relatively equivalent bundles and then a unique midcell pattern with unequally sized bundles (Figures 3F and S5E). These more complex patterns could reflect intermediate stages in the evolution of mother/sister/sister nucleoid relationships.

Time Series at 5 s Intervals Reveal Elongation-Biased Density Waves Plus Coalescence of New Material into Existing Longitudinal Density Bundles

Longitudinal density waves underlie nucleoid elongation. In roughly half of all 5 s time series, a significant increase in overall nucleoid length can be detected over the 1–2 min visualization window, and all of these cases exhibit dynamic fluxing of density toward one or both ends of the nucleoid (e.g., Figure 3C). In favorable cases, e.g., when there is significant "space" at the end of the cell, specific morphological details can be discerned, as in Figure 3G. Here, a protrusion emerges from the new pole end of the nucleoid into previously unoccupied space, then retracts, then protrudes, and then retracts cyclically, with net forward extension analogous to an incoming tide (blue arrows, Figure 3G, i and ii). Each protrusion is the leading edge of a longitudinal density wave that fluxes through the shape toward the growing end (red arrows, Figure 3G, i).

Furthermore, at a suitable isointensity threshold, dual longitudinal density bundles can be seen within the protruding material, fluctuating between tightly juxtaposed and open configurations as seen on a larger scale (above). Most importantly, these bundles evolve by coalescence of the fluxing material into pre-existing bundles: as a wave of density moves toward the growing end, it is efficiently incorporated into existing bundles to give smooth elongation of the shape.

The occasional nucleoid exhibits an extremely thin protrusion that curves progressively around the radial cell periphery with concomitant fluxes of density along its length (Figure 3H and Movie S6). These and other images (e.g., Figures 3G and S2E) suggest that the structure is capable of exploring space and, together with post-G1 nucleoids showing "space" at the end of the cell (e.g., Figures 3B, S2A and S2F), confirm that the helical shape does not arise by pushing of the nucleoid up against the end of the cell.

The Post-G1 Nucleoid Elongates Discontinuously via Sequential Pulses that Occur at Defined Times in the Cell Cycle

Time-lapse analyses with 3D images of a single nucleoid are collected at 1 min intervals revealing a striking, unanticipated behavior: the *E. coli* nucleoid elongates discontinuously over time. Approximately 10 min pulses of rapid length increase occur approximately every 20 min, as seen in primary length curves and changes in the rate of nucleoid length increase (Figure 4A, top and bottom). On average, in each pulse, nucleoid length increases ~200 nm, or ~5%–15% of nucleoid length. In contrast, end-to-end cell length increases monotonically over time throughout the cell cycle (Figure S6). Interestingly, a period of length increase is usually preceded by a short period of nucleoid shortening (Figure 4A, top) and a corresponding negative rate of length increase (Figure 4A, bottom), suggesting that

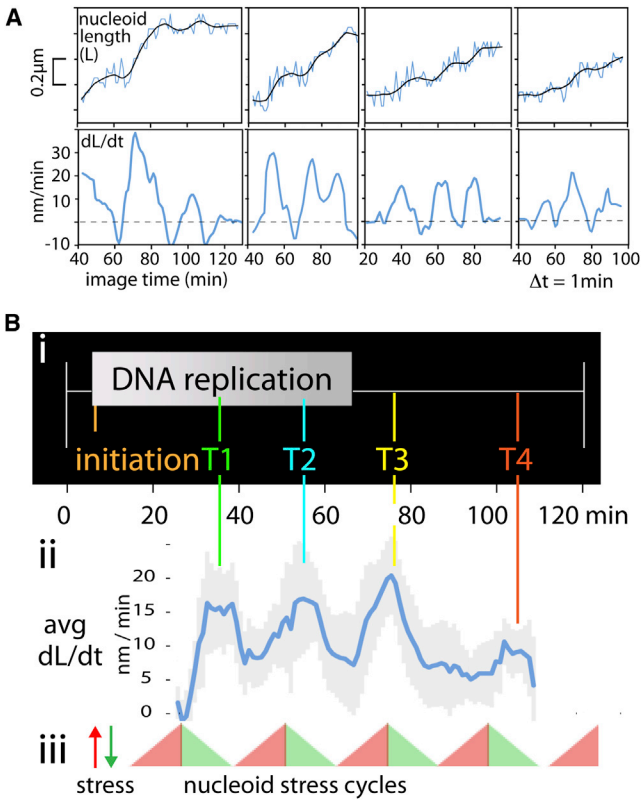

Figure 4. The Nucleoid Elongates in 10 min Pulses at Defined 20 min Intervals during the Cell Cycle

(A) Lengths of four individual nucleoids, imaged at successive 1 min intervals, show pulses of increase, usually immediately preceded by a short period of nucleoid shortening, as seen in primary length curves (top) and rates of increase given by the slopes of those curves (bottom). In contrast, cell length increases monotonically throughout (Figure S6).

(B) (i and ii) Averaging of rate increases for multiple data sets (N = 14) reveals that pulses of length increase occur at 20 min intervals, at specific times through the analyzed period of the cell cycle, in temporal correlation with the times of the T1–T4 transitions. For each minute in the cell cycle, the sliding window average (blue line) and the corresponding standard deviation (grey shadow) are shown. (iii) Pulses could correspond to periodic accumulation and release of nucleoid stress.

elongation is immediately preceded by a global change of internal nucleoid state.

When multiple data sets (n = 14) are aligned with respect to cell-cycle timing and nucleoid elongation rates averaged over time, it further emerges that pulses of nucleoid elongation occur at specific times in the cell cycle. Maximum elongation rates are similar in each period (15–20 nm/min; Figure 4B, ii). The ~100 min period analyzed, which extends from early-mid DNA replication to ~40 min after the end of replication, exhibits four sequential length increase pulses. Since the last two pulses occur at the end of, and well after, DNA replication, respectively, these pulses are independent of concomitant replication.

We infer that, during each ~10 min period of nucleoid length increase, elongation is implemented by the sum of many short-timescale longitudinal density waves. For example, the sequence of waves and length increases defined by imaging at 5 s intervals in Figure 3G presumably represents ~40 s out of a ~10 min elongation period.

Tether-Mediated Sister-Separation Transitions Are Temporally and Morphologically Correlated with Nucleoid Elongation Pulses

A further striking finding is that the cell-cycle times of the four pulses of nucleoid elongation match the times of four previously described nucleoid transitions, each of which corresponds to a discrete increase in global and/or local sister separation and has either been shown, or is suspected, to involve release of one or more programmed tethers that would constrain separation (Figure 4B, i and ii; Bates et al., 2005; Joshi et al., 2011). Real-time analysis confirms that temporal correspondence is accompanied by direct morphological correspondences.

Background

Transitions T1–T4 are each characterized by increased sister separateness for *oriC* (T1/T2) or the terminus region (*ter*) (T3/T4) (Figure 5A) (Bates et al., 2005; Joshi et al., 2011). The best-studied transition, T2, is a global nucleoid reorganization that additionally includes (1) a discrete increase in the separateness of sister loci throughout the genome; (2) appearance of strongly bilobed nucleoid morphology, with one sister locus in each lobe; and (3) movement of the terminus region inward toward midcell (Bates et al., 2005; Joshi et al., 2011). A subtler global increase in sister separateness occurs at T1. Such data permit a specific model for sister/mother dynamics (Figure 5B, left): DNA replication initiates at a position toward one end of the nucleoid (A.B., unpublished data). At T1, one sister domain moves toward one cell pole, away from the mother nucleoid, leaving the other sister domain near midcell, proximal to the mother domain. At T2, the midcell sister domain moves to the other cell pole, switching places with the mother domain, which moves inward (along with *ter*). Sister *oriC* movements match this pattern (Figures 5A and 5B, right). T3 is defined by splitting sister *ter*s, which remain at the edge of one nucleoid lobe. At T4, separated sister *ter*s move to the inner edges of sister nucleoids (Figure 5A).

T1 involves sequential release of two programmed tethers that link, respectively, sister oriCs and leftward and rightward replisomes (Figure 5C, top). The two release steps occur ~5 min apart (Bates and Kleckner, 2005; D. Bates, personal communication). T2 involves a unique set of intersister "snaps" in the right replichore where sisters remain cohered much longer than at intervening and flanking loci (Figure 5C, bottom) (Bates et al., 2005; Joshi et al., 2011). Moreover, even though snap loci are nonadjacent, they undergo sister splitting coordinately at T2. T3 involves loss of linkage between sister *ter*s. T4 could involve release of any of several other known terminus-region tethers.

Stepwise Emergence of Bilobed Nucleoid Morphology at T1–T4

Bilobed nucleoid morphology evolves in discrete steps corresponding to the T1–T4 transitions; thus, all four transitions result in increased global separation of sister domains, as known for T2.

Bilobed character, defined in Z projections, corresponds to a tendency for the longitudinal intensity distribution to exhibit two peaks separated by a valley (Figure 5D, left). Analysis of

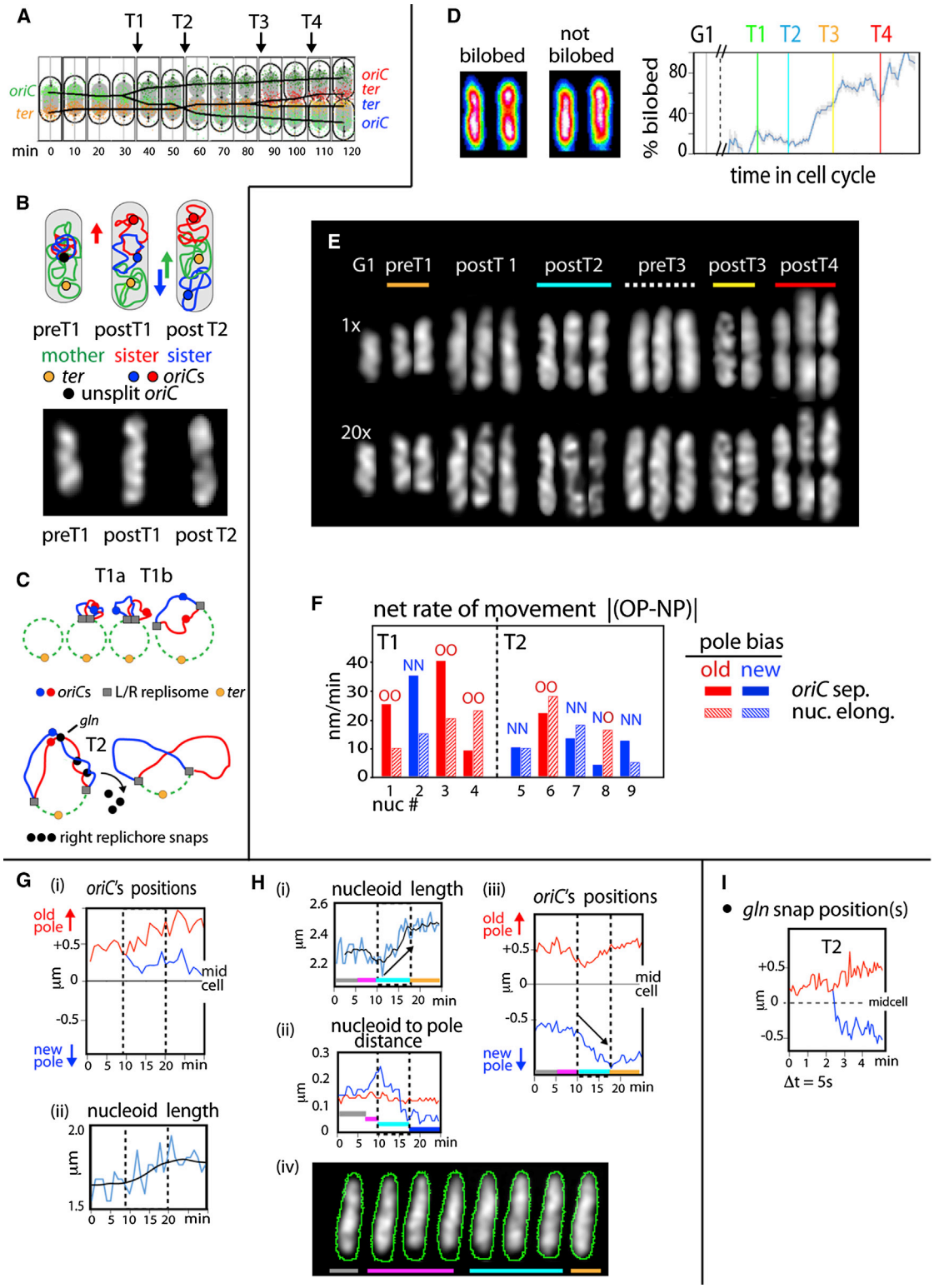

Figure 5. Nucleoid Elongation Pulses Correspond to Global Increases in Sister Separation

(A) T1–T4 transitions as previously described (Bates and Kleckner 2005; Joshi et al., 2011; Results).

(B) Top: model for spatial evolution of sister and mother regions via T1 and T2 transitions (Joshi et al., 2011). Bottom: matching whole-nucleoid images occur at appropriate stages.

(C) Programmed tethers that modulate T1 and T2 (Joshi et al., 2011; Results).

(legend continued on next page)

more than 1,000 nucleoids representing times throughout the cell cycle shows that probability of bilobed character increases during the cell cycle in good correspondence to the four transitions: negligible before T1; low but significant from T1 to T2 onset; dramatically increased at and after T2; and further increased at T3 and again at T4 (Figure 5D, right).

Additionally, nucleoid morphologies have been analyzed in hundreds of 3D time series, with images taken at intervals ranging from 5 s to 10 min. Despite dynamic variations, certain pronounced morphologies occur uniquely at certain specific periods and document a stepwise increase in bilobed character (Figure 5E). (1) Following T1, nucleoids can exhibit a terminal projection or "bud," usually at the old pole end of the cell. (2) Following T2, nucleoids can exhibit two lobes of similar size, less or more distinct, and linked by substantial intervening material. (3) Following T3, the tendencies seen at T2 become more pronounced, with larger separation between the two lobes. (4) Following T4, the tendencies seen after T2 and T3 continue, with sisters finally linked only by a thin thread. Notably, T1 and T2 morphologies match those predicted by the proposed model (Figure 5B, bottom; left versus right).

Remarkably and unexpectedly, immediately prior to T3, the probability of bilobed character diminishes and essentially single continuous shapes can be seen (Figures 5D and 3F). An analogous effect may occur prior to T2. Apparently, during periods when sister separation is slowed or stalled, awaiting release of the next set of tethers, density fills in the region between already-separating lobes to give a single continuous shape. Then, upon tether release, duality re-emerges in a more pronounced state than before. This same alternation of morphologies is also seen in snapshots of individual living cells from large synchronous populations imaged under different conditions.

Thus, nucleoid elongation during the T1–T4 period reflects progressive increases in the end-to-end separation of sister domains, which is alternately impeded by constraining tethers and then licensed by tether release.

At T1 and T2, Sequentially Separating Sister oriCs Are Carried in Opposite Directions on Sequential Pulses of Nucleoid Elongation

Individual nucleoids were examined for the relative rates at which sister origins move toward their respective poles during periods of nucleoid length increase (Figure 5F, closed bars). At T1, the origin moving toward the old pole of the cell usually moved faster than the origin moving toward the new pole (Figure 5F, closed red bars). At T2, oppositely, the origin moving toward the new pole of the cell moved faster than the origin moving toward the old pole (Figure 5F, closed blue bars). Moreover, the magnitude of the difference in rate of movement was less for T2 than for T1, in accordance with the fact that the lagging origin had already previously carried out some of its poleward movement during T1 (Figure 5A).

Furthermore, in these same cells, nucleoid elongation occurs with the same sequential directional bias as *oriC* movement. The nucleoid usually elongates more rapidly toward the old pole at T1 and more rapidly toward the new pole at T2 (Figure 5F, red and blue hatched bars; other examples in Figures 3G and 3H). Correspondingly, *oriC* and nucleoid directionality exhibit the same directional bias on a per-nucleoid basis, in eight out of nine examined cases (Figure 5F, OO and NN). In essence, *oriC*s are riding along with the differential elongation of the nucleoid, first in one direction and then in the other.

Correspondingly, despite considerable diversity, some nucleoids exhibit the prototypical "population average" pattern for T1 or T2 movements. Figure 5G shows a T1 nucleoid: following splitting of sister origins, one *oriC* moves steadily to the old pole, whereas its sister, after an initial separation, shows little net movement. Figure 5H shows a T2 nucleoid: a cycle of nucleoid shortening is followed by nucleoid lengthening, both occurring specifically at the new pole end of the cell (Figure 5H, i, ii, and iv) and accompanied by differential movement of the new pole-proximal *oriC* toward its pole (Figure 5H, iii).

These patterns, in toto, directly link increased separation of sister *oriC*s, and their underlying sister domains, to pulses of nucleoid elongation and confirm the evolution of sister-mother relationships at T1 and T2 via sequential movement of sister domains in opposite directions (Figure 5C).

Tethers Are under Tension prior to Splitting

Real-time analysis of tether release at one T2 snap locus, *gln* (Figure 5C), shows that splitting of sister *gln* loci is accompanied by very rapid movement of one *gln* locus (400 ± 131 nm/min; N = 3), specifically toward the new pole end of the nucleoid; in contrast, the other *gln* locus changes little in net position (e.g., Figure 5I). This behavior strongly suggests that intact intersister tethers are under tension due to the ongoing, but constrained, tendency for movement of one sister domain toward the new pole end of the cell (Figure 5B) and that, upon release of the

(D) Bilobed character was defined for more than 1,000 nucleoids from known times throughout the cell cycle by analysis of longitudinal density distributions in Z projections. Left: examples of bilobed and nonbilobed states. Right: Frequency of nucleoids showing bilobed character increases in discrete steps at the T1–T4 transitions.

(E) Pronounced nucleoid morphologies characteristic of the indicated stages. Midplanes from 1 × deconvolved and 20 × deconvolved images (top and bottom).

(F) Sister *oriC*s usually exhibit differential separation toward the old pole (filled red bars) and new pole (filled blue bars) at the T1 and T2 transitions, respectively. y axis = Δ = |(rate of increase toward old pole − rate of increase toward new pole)|. Bias is more pronounced at T1 versus T2: Δ = 28 nm/min (± 1.4) and 12 nm/min (± 6.5), respectively. Concomitant nucleoid length increases (hatched bars) occur differentially in the same direction as *oriC* movement in 4/4 T1 nucleoids and 4/5 T2 nucleoids.

(G) A T1 nucleoid imaged at 1 min intervals. *oriC* separates differentially toward the old pole (i) during a pulse of nucleoid length increase (ii) that also occurs preferentially toward the old pole end of the cell (not shown).

(H) A T2 nucleoid, imaged at 30 s intervals. (i) A pulse of length increase (turquoise) preceded by a period of nucleoid shortening (pink). (ii) Nucleoid length increases toward the new pole end of the cell (turquoise). (iii) Concomitant differential movement of the midcell sister *oriC* toward the new pole end at 50 nm/min (turquoise).

(I) Separation of sisters at the T2 "snap" locus *gln*, defined by 2D imaging at 5 s intervals. Loci separate at approximately 380 nm/min, significantly faster than *oriC* splitting at T1 or T2.

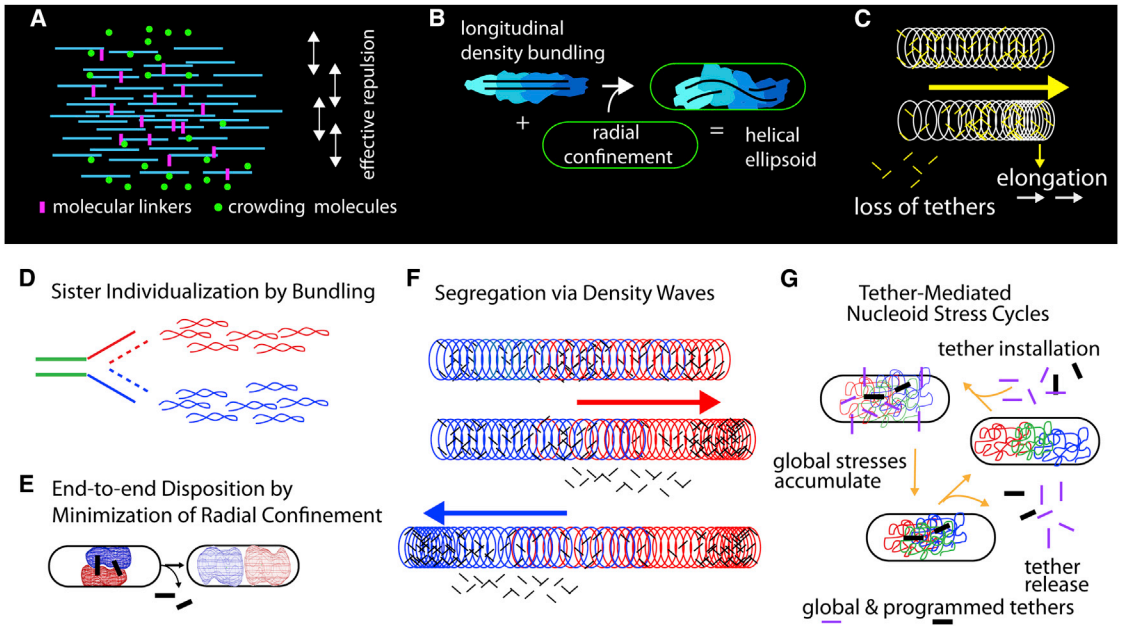

Figure 6. *E. Coli* Nucleoid Shape, Organization, and Dynamics

(A) Longitudinal density bundles could comprise subbundles (e.g., supercoiled plectonemes). Association via weak forces, to permit ready adjustment, could reflect molecular crowding and/or weak-binding linker proteins. Associative effects of bundling could be opposed by an effective repulsion to give low DNA density.

(B) Longitudinal density bundles create ellipsoid shape that is helically deformed by interaction with the cell periphery (radial confinement).

(C) Longitudinal density waves tend to promote release of tethers at the lagging end. Given directionality, they can underlie elongation at the leading end.

(D–F) Sister segregation without a spindle.

(D) Genomically biased longitudinal bundling promotes individualization of sisters into distinct units.

(E) Minimization of radial-confinement stress promotes placement of sister units in an end-to-end disposition versus other relationships.

(F) The back-and-forth motion of density waves facilitate sister segregation by "greasing" the system, removing constraining linkages to increase mobility.

(G) Global tether-mediated nucleoid-stress cycles (Discussion).

tether, the corresponding snap locus undergoes rapid elastic retraction into its already-separating domain.

DISCUSSION

The presented results define *E. coli* nucleoid organization, shape, and short- and long- timescale dynamics in living cells. Four basic features emerge: longitudinal density bundling, radial confinement, longitudinal density waves, and modulation of sister segregation by programmed intersister tethers. The central role of radial confinement, plus the effects of tethers, suggest that the system can be viewed in mechanical terms, with physical features and effects playing critical governing roles. Taken together, the observed results provide a coherent conceptual framework for understanding and for further analysis of nucleoid morphology, morphogenesis, and dynamics, including segregation of sister chromosomes.

Nucleoid Shape and State

The nucleoid is revealed to be a discrete, internally organized object. Internal organization comprises longitudinal density bundles that intrinsically tend to be dual (or, more generally, split), irrespective of genomic connectivity. Since bundle patterns are dynamic, involved associative forces are relatively weak. Physical effects (e.g., protein-mediated molecular crowding [Cunha et al., 2001; Adams and Fraden, 1998]) and/or weak molecular linking interactions (reviewed in Reyes-Lamothe et al., 2008) are possibilities; negatively supercoiled plectonemes are probably involved (Figure 6A).

Importantly, virtually all nucleoid material is contained within the shape, implying a strong tendency for coalescence. On the other hand, the density of DNA atoms is very low, comprising less than 2% of total nucleoid volume. Thus, coalescence into bundles is probably opposed by an effective repulsion. Together these features create a stiff, springy shape. Repulsion could reflect physical effects (excluding volume [Wiggins et al., 2010] or charge), and/or biochemical effects (e.g., a diffusion ratchet; Vecchiarelli et al., 2010).

The nucleoidal ellipsoid has a helix-like shape. This shape results from deformation of the ellipsoid by radial confinement (Figure 6B). This feature implies that the longitudinal persistence length of the ellipsoid is greater than the radius of the confining cell cylinder. Correspondingly, progressive evolution of helical nucleoid(s) during the cell cycle can reflect extension of existing helical path(s) by coalescence of material into stiff longitudinal bundles.

These results confirm and extend previous evidence for internal organization (Odijk, 1998; Cunha et al., 2001), nucleoid

stiffness (Wiggins et al., 2010), and/or helix-like shape (Hadizadeh Yazdi et al., 2012). They exclude models in which the nucleoid is a randomly oriented polymer whose shape is defined by the cell cylinder (Jun and Mulder, 2006) or where helical shape arises by the pushing of a linear object up against the cell pole(s) (e.g., Wiggins et al., 2010; Jun and Mulder, 2006; Chaudhuri and Mulder, 2012).

Replication-Independent Longitudinal Density Waves Mediate Chromosome Mobility

Waves of nucleoid density flux longitudinally, back and forth, along the helical path of the shape, over distances comparable to the length of the nucleoid. Our preliminary qualitative impression is that the waves of density are likely to be oscillatory, with longer timescale periodicities of the order of a minute. Since fluxes result in only small net changes in density distribution, we infer that they involve subtle changes in fiber proximities (Figure 6C) rather than global, coherent nucleoid movement.

Longitudinal density waves are independent of ongoing DNA replication. They may involve an active ATP-driven biochemical process because they are highly dynamic; in contrast, thermal adjustments, which involve low energies, tend to be slow. Nucleoid dynamics are known to be strongly ATP modulated (Weber et al., 2012).

The nature of density waves suggests that their general role is to promote mobility within the nucleoid (Figure 6C). As a wave passes, increased nucleoid density at the leading end will be accompanied by decreased nucleoid density at the lagging end. This, in turn, will tend to reduce constraining interfiber linkages (e.g., by disfavoring rebinding of dissociating unstable linker molecules). This effect will destabilize unwanted linkages that impede all types of nucleoid dynamics. The need to reduce nonspecific meshwork linkages is a notable, not often emphasized, concern. Many chromosomal molecules nonspecifically link pairs of DNA segments (Reyes-Lamothe et al., 2008). Linkages *along* a chromosome fiber could play positive roles (e.g., as organizational loops); however, linkages between unrelated segments will tend to create an immobile gel incompatible with both global and local dynamics. The need for elimination of spontaneous meshwork linkages and the ability of density waves to accomplish this task could be important general features of chromosome biology.

Global Dynamics and Segregation of Sisters without a Spindle

Taken together, the above-described nucleoid features, plus programmed and nonspecific intranucleoid tethers, can explain global nucleoid dynamics, including sister segregation.

Individualization

Longitudinal density bundling will promote individualization of sister chromosomes into their respective discrete units. As sisters emerge from the replication fork, bundling of adjacent positions along the same sister will be intrinsically favored over bundling of segments on different sisters (Figure 6D). Thus, at this stage (contrary to G1), bundling will be genomically biased but will be further sharpened by the intrinsic tendency for bundle duality. Complex bundle patterns at intermediate stages would thus reflect the simultaneous presence of bundles corresponding to the mother and two sister domains.

Minimization of Radial Confinement

Radial confinement is a nonequilibrium, high-energy (mechanically stressed) condition. Given two individualizing sister units, minimization of radial-confinement stress will drive and direct these units into an end-to-end configuration, versus a longitudinally overlapping state, because radial-confinement stress will be much reduced in the former state relative to the latter (Figure 6E). Radial-confinement stress (and thus segregation force) will increase due to synthesis of new material during DNA replication, but probably is also modulated in other ways, as discussed further below. Minimization of radial-confinement stress would thus be the functional bacterial analog of eukaryotic mitotic spindle forces, promoting spatial separation as required for regular cell division.

More generally, minimization of radial confinement can provide a driving force and a directionality for all global nucleoid dynamics. For example, the two observed G1 changes—elongation and development of a more symmetrical shape—are those required to reduce radial-confinement stress.

Longitudinal Density waves

Longitudinal density waves will facilitate sister segregation by "greasing" the process, increasing nucleoid mobility to permit implementation of confinement-driven changes in sister disposition (Figure 6F). Density waves will similarly facilitate global G1 adjustments.

This three-component model for sister segregation accommodates our previous suggestion that sisters separate by intersister pushing (Bates and Kleckner, 2005). It differs qualitatively from other models (Introduction) because (1) individualization of sisters is a specific feature, not simply a secondary consequence of spatial separation of chromosome fibers; (2) end-to-end disposition arises from pushing forces and involves evolution of coherent domains, rather than arising from pulling forces exerted on centromere-like loci; and/or (3) no intracellular scaffolds or peripheral cytoskeletal "railroad tracks" are involved.

Generality

The basic features and processes described above for the *E. coli* nucleoid could apply to other bacteria as well. With respect to nucleoid shape and state, *B. subtilis* nucleoids exhibit an analogous progression of helical shapes (Berlatzky et al., 2008) and a linear *E.coli*-like genome organization (D. Rudner, personal communication). Also, the Caulobacter G1 nucleoid is a ~1.5-turn helical ellipsoid with dual longitudinal density bundles (Umbarger et al., 2011). In that case, due to polar tethering of *ori* and *ter*, bundle formation is biased by genomic connectivity such that the two bundles correspond to left and right replichores. Interestingly, helical shape provides a continuous lower-density complementary space through which larger objects can freely move, which could accommodate rapid movement of one sister *oriC* from its original pole to the opposite end of the cell.

Three-component sister segregation could also occur in all rod-shaped bacteria. This idea is at odds with current views of Caulobacter segregation, often envisioned to involve polar *oriC*

localization and replication-linked compaction toward the two cell poles. However, it is possible to envision collaboration between molecularly promoted *oriC* localization and the types of physical effects described here, in both (all) organisms.

This model for segregation can also explain why bacteria occur only in three basic shapes—rods, spirals, and spheres. Well-individualized chromosomes in a confined space will always position themselves into their lowest energy state, which will be the one that minimizes overlap. For a rod or a spiral, that state is end-to-end disposition. For a sphere of small-enough radius, a pair of fat ellipsoidal nucleoids will be in a symmetrical disposition, also suitable for segregation.

Moreover, the same scenario could explain both sister segregation and cell division in evolving life: individualization will confer sister separateness; minimization of overlap in a confining membrane protocell will place the sisters in a regular relationship; and the need for separateness under confinement would create mechanical weak points at the internucleoid boundaries, giving a primordial mechanism that provokes cell division at the appropriate positions.

Cyclic Release of Programmed and Nonspecific Tethers

End-to-end segregation of sister chromosomes evolves in discrete steps as mediated by programmed tethers. T1 and T2 probably promote regular sister nucleoid disposition: basic *ori*-centric orientation is set up for one sister at (T1), thus simplifying events at the major separation transition (T2). T2 concomitantly brings the terminus region into juxtaposition for capture at midcell, where T3 and T4 mediate ensuing *ter*-related events.

If sister segregation is driven by minimization of radial confinement stress, and since programmed tethers are under mechanical tension at the time of their release, tether-mediated sister-separation cycles are most simply explained by cyclic accumulation and release of radial-confinement stress (Figure 4B, iii). However, several factors point to the existence of more general global nucleoid stress cycles, with sister segregation superimposed as one outcome. (1) T3 and T4 occur after completion of DNA replication, implying that ongoing replication-generated increase in radial-confinement stress is not required. (2) At T4, sister nucleoids are already well separated, so the source of nucleoid stress might not be sister overlap. (3) Each transition is preceded by a tendency for nucleoid shortening, implying global changes in state throughout the nucleoid. (4) Cycles may occur at all times: nucleoid release from midcell and ensuing relaxation at G1 could comprise a prereplicative cycle and preliminary results hint at an additional post-T4 cycle.

We propose that pulses of nucleoid length increase reflect the accumulation and release of intranucleoid stress mediated globally by nonspecific tethers (Figure 6E). Basic chromosome metabolism would provoke chromosome fiber changes whose realization is constrained by the tether meshwork, despite the counteracting effects of longitudinal density waves. The result would be accumulation of an unfavorable (stressed) state along the fiber and, concomitantly, via increased radial confinement. When stress reaches a critical level it will provoke catastrophic release of meshwork tethers (and, concomitantly, programmed tethers) thus licensing a more relaxed state. By this scenario, a fundamental role of the observed pulses would be to periodically "cleanse" the genome of unwanted linkages, in addition to promoting specific programmed transitions. An obvious candidate for altered stress would be supercoiling, whose dynamically and regionally modulated level is, in turn, determined primarily by transcription (Rovinskiy et al., 2012).

The observed cycles essentially comprise a primordial cell cycle. Interestingly, eukaryotic organisms also undergo cyclic expansion and compaction of chromatin (Kleckner et al., 2004). It is not excluded that the two types of cycles correspond and that the chromatin stress cycle predates, and now works in parallel linkage with, the cell-cycle engine.

Synthesis

The presented results provide a coherent, general conceptual framework for understanding bacterial nucleoid morphogenesis and dynamics, including, but not limited to sister segregation. The central feature of this framework, which distinguishes it from previous considerations, is that the nucleoid is considered as a complex and evolving, but coherent, object whose intrinsic mechanical features play critical governing roles. Underlying basic effects can thus be described in mechanical terms, rather than in the language of molecular biology, biochemistry, or DNA topology.

EXPERIMENTAL PROCEDURES

Microbiology

Except as noted (Extended Experimental Procedures), studies used CM735-derived strain NK9386 (Bates et al., 2005) expressing *hupA::mCherry* (Marceau et al., 2011), plasmid-borne pBAD-TetR-mVenus (Wang et al., 2005), and an *asnA::tetO* (Lau et al., 2003) or *gln::tetO* (Joshi et al., 2011) array. Growth conditions were as described (Bates and Kleckner 2005; Joshi et al., 2011; Bates et al., 2005).

Microfluidics

Cells were imaged in a microfabricated Polydimethylsiloxane (PDMS) device (Whitesides 2006; Figures 1A, top, and S1A). Cells are injected at a high flow rate, which causes growth channels to expand slightly, after which the flow rate is reduced, gently trapping cells between the PDMS upper surface and the glass coverslip bottom surface (Figure 1A). Thereafter, fresh medium flowed through the channels at 0.7 ml/hr with temperature maintained at 30°C (Extended Experimental Procedures).

3D Microscopy

Z section slice separation ranged from 45–200 nm with 100–300 ms exposure time per slice and typically covered a range of 1.2 μm. Three-dimensional data sets were deconvolved using the blind deconvolution algorithm of AutoQuant (Media Cybernetics, Inc.) with the Point Spread Function appropriate to our microscope (Extended Experimental Procedures) at each emission wavelength.

Further processing was done using ImageJ software (National Institutes of Health), MatLab, and Pymol (http://www.pymolwiki.org/index.php/Tiff2ccp4; D. Jeruzalmi and J. Vertrees). All analyses (3D rendering of nucleoid data sets, definition and analysis of cell boundaries from midplane phase-contrast images, transformation of Z stacks into a series of (XZ) slices along the length of the nucleoid in the Y dimension, calculation of density centroid paths, Z projections, pseudocolor mapping, quantification of longitudinal density fluxes, determination of bilobed nucleoid character, localization of FROS foci, and detailed protocols for dynamics analyses are described in Extended Experimental Procedures.

SUPPLEMENTAL INFORMATION

Supplemental Information includes six figures, six movies, and Extended Experimental Procedures and can be found with this article online at http://dx.doi.org/10.1016/j.cell.2013.04.006.

ACKNOWLEDGMENTS

We thank G. Guidotti, K. Mizuuchi, E. Garner, and Kleckner laboratory members for helpful comments; D. Jeruzalmi and J. Vertrees for adaptation of PyMOL to nucleoid images; and R. Johnson for a FIS-GFP plasmid. Research was supported by NIH grant NIH/NIGMS-R01-GM025326 to N.K. and Swiss National Science Foundation grant PBELP3-135860 to G.W. We acknowledge the Center for Computer Integrated Systems for Microscopy and Manipulation at UNC Chapel Hill, funded by NIH grant NIBEB-5-P41-EB002025, and the Center for Nanoscale Systems (CNS) at Harvard University, a member of the National Nanotechnology Infrastructure Network.

Received: September 28, 2012
Revised: March 6, 2013
Accepted: March 27, 2013
Published: April 25, 2013

REFERENCES

Adams, M., and Fraden, S. (1998). Phase behavior of mixtures of rods (tobacco mosaic virus) and spheres (polyethylene oxide, bovine serum albumin). Biophys. J. *74*, 669–677.

Banigan, E.J., Gelbart, M.A., Gitai, Z., Wingreen, N.S., and Liu, A.J. (2011). Filament depolymerization can explain chromosome pulling during bacterial mitosis. PLoS Comput. Biol. *7*, e1002145.

Bates, D. (2008). The bacterial replisome: back on track? Mol. Microbiol. *69*, 1341–1348.

Bates, D., and Kleckner, N. (2005). Chromosome and replisome dynamics in *E. coli*: Loss of sister cohesion triggers global chromosome movement and mediates chromosome segregation. Cell *121*, 1–13.

Bates, D., Epstein, J., Boye, E., Fahrner, K., Berg, H., and Kleckner, N. (2005). The *Escherichia coli* baby cell column: a novel cell synchronization method provides new insight into the bacterial cell cycle. Mol. Microbiol. *57*, 380–391.

Berlatzky, I.A., Rouvinski, A., and Ben-Yehuda, S. (2008). Spatial organization of a replicating bacterial chromosome. Proc. Natl. Acad. Sci. USA *105*, 14136–14140.

Chaudhuri, D., and Mulder, B.M. (2012). Spontaneous helicity of a polymer with side loops confined to a cylinder. Phys. Rev. Lett. *108*, 268305.

Cunha, S., Woldringh, C.L., and Odijk, T. (2001). Polymer-mediated compaction and internal dynamics of isolated *Escherichia coli* nucleoids. J. Struct. Biol. *136*, 53–66.

Espéli, O., Borne, R., Dupaigne, P., Thiel, A., Gigant, E., Mercier, R., and Boccard, F. (2012). A MatP-divisome interaction coordinates chromosome segregation with cell division in *E. coli*. EMBO J. *31*, 3198–3211.

Hadizadeh Yazdi, N., Guet, C.C., Johnson, R.C., and Marko, J.F. (2012). Variation of the folding and dynamics of the *Escherichia coli* chromosome with growth conditions. Mol. Microbiol. *86*, 1318–1333.

Joshi, M.C., Bourniquel, A., Fisher, J., Ho, B.T., Magnan, D., Kleckner, N., and Bates, D. (2011). *Escherichia coli* sister chromosome separation includes an abrupt global transition with concomitant release of late-splitting intersister snaps. Proc. Natl. Acad. Sci. USA *108*, 2765–2770.

Jun, S., and Mulder, B. (2006). Entropy-driven spatial organization of highly confined polymers: lessons for the bacterial chromosome. Proc. Natl. Acad. Sci. USA *103*, 12388–12393.

Kleckner, N., Zickler, D., Jones, G.H., Dekker, J., Padmore, R., Henle, J., and Hutchinson, J. (2004). A mechanical basis for chromosome function. Proc. Natl. Acad. Sci. USA *101*, 12592–12597.

Kuhlman, T.E., and Cox, E.C. (2012). Gene location and DNA density determine transcription factor distributions in *Escherichia coli*. Mol. Syst. Biol. *8*, 610.

Lau, I.F., Filipe, S.R., Søballe, B., Økstad, O.A., Barre, F.X., and Sherratt, D.J. (2003). Spatial and temporal organization of replicating *Escherichia coli* chromosomes. Mol. Microbiol. *49*, 731–743.

Lemon, K.P., and Grossman, A.D. (2001). The extrusion-capture model for chromosome partitioning in bacteria. Genes Dev. *15*, 2031–2041.

Marceau, A.H., Bahng, S., Massoni, S.C., George, N.P., Sandler, S.J., Marians, K.J., and Keck, J.L. (2011). Structure of the SSB-DNA polymerase III interface and its role in DNA replication. EMBO J. *30*, 4236–4247.

Norris, V. (1995). Hypothesis: chromosome separation in *Escherichia coli* involves autocatalytic gene expression, transertion and membrane-domain formation. Mol. Microbiol. *16*, 1051–1057.

Odijk, T. (1998). Osmotic compaction of supercoiled DNA into a bacterial nucleoid. Biophys. Chem. *73*, 23–29.

Reyes-Lamothe, R., Wang, X., and Sherratt, D.J. (2008). *Escherichia coli* and its chromosome. Trends Microbiol. *16*, 238–245.

Rovinskiy, N., Agbleke, A.A., Chesnokova, O., Pang, Z., and Higgins, N.P. (2012). Rates of gyrase supercoiling and transcription elongation control supercoil density in a bacterial chromosome. PLoS Genet. *8*, e1002845.

Swulius, M.T., and Jensen, G.J. (2012). The helical MreB cytoskeleton in *E. coli* MC1000/pLE7 is an artifact of the N-terminal YFP tag. J. Bacteriol. *194*, 6382–6386.

Toro, E., and Shapiro, L. (2010). Bacterial chromosome organization and segregation. Cold Spring Harb. Perspect. Biol. *2*, a000349.

Toro, E., Hong, S.H., McAdams, H.H., and Shapiro, L. (2008). Caulobacter requires a dedicated mechanism to initiate chromosome segregation. Proc. Natl. Acad. Sci. USA *105*, 15435–15440.

Umbarger, M.A., Toro, E., Wright, M.A., Porreca, G.J., Baù, D., Hong, S.H., Fero, M.J., Zhu, L.J., Marti-Renom, M.A., McAdams, H.H., et al. (2011). The three-dimensional architecture of a bacterial genome and its alteration by genetic perturbation. Mol. Cell *44*, 252–264.

Vecchiarelli, A.G., Han, Y.W., Tan, X., Mizuuchi, M., Ghirlando, R., Biertümpfel, C., Funnell, B.E., and Mizuuchi, K. (2010). ATP control of dynamic P1 ParA-DNA interactions: a key role for the nucleoid in plasmid partition. Mol. Microbiol. *78*, 78–91.

Wang, X., Possoz, C., and Sherratt, D.J. (2005). Dancing around the divisome: asymmetric chromosome segregation in *Escherichia coli*. Genes Dev. *19*, 2367–2377.

Wang, X., Liu, X., Possoz, C., and Sherratt, D.J. (2006). The two *Escherichia coli* chromosome arms locate to separate cell halves. Genes Dev. *20*, 1727–1731.

Wang, W., Li, G.W., Chen, C., Xie, X.S., and Zhuang, X. (2011). Chromosome organization by a nucleoid-associated protein in live bacteria. Science *333*, 1445–1449.

Weber, S.C., Spakowitz, A.J., and Theriot, J.A. (2012). Nonthermal ATP-dependent fluctuations contribute to the in vivo motion of chromosomal loci. Proc. Natl. Acad. Sci. USA *109*, 7338–7343.

Whitesides, G.M. (2006). The origins and the future of microfluidics. Nature *442*, 368–373.

Wiggins, P.A., Cheveralls, K.C., Martin, J.S., Lintner, R., and Kondev, J. (2010). Strong intranucleoid interactions organize the *Escherichia coli* chromosome into a nucleoid filament. Proc. Natl. Acad. Sci. USA *107*, 4991–4995.